Cell Reports

Unique potential of immature adult-born neurons for the remodeling of CA3 spatial maps

Graphical abstract

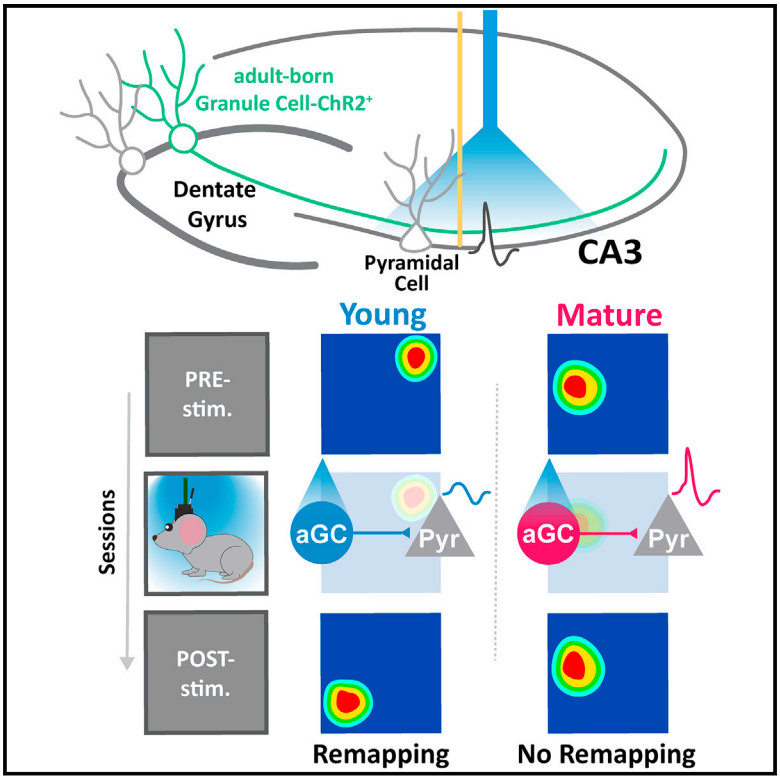

Authors

Matías Mugnaini, Mariela F. Trinchero, Alejandro F. Schinder, Verónica C. Piatti, Emilio Kropff

Correspondence

aschinder@leloir.org.ar (A.F.S.), vpiatti@leloir.org.ar (V.C.P.), ekropff@leloir.org.ar (E.K.)

In brief

Mugnaini et al. examine the ability of young vs. mature neurons to change CA3 spatial representations. Adult-born cells can update CA3 maps when they are young and their post-synaptic network recruitment is low. This form of plasticity could be key to understanding the function of adult mammalian neurogenesis.

Highlights

- Immature aGCs induce place cell remapping in CA3 while rarely evoking spiking activity
- Remapping cells transiently lose stability, exhibiting new stable spatial maps 24 h later
- Further stimulation induces no remapping but recruits a larger CA3 population
- This potential to remodel CA3 representations is lost with aGC maturation

Mugnaini et al., 2023, Cell Reports *42*, 113086
September 26, 2023
https://doi.org/10.1016/j.celrep.2023.113086

CellPress

Cell Reports

CellPress
OPEN ACCESS

Report

Unique potential of immature adult-born neurons for the remodeling of CA3 spatial maps

Matías Mugnaini,[1,2] Mariela F. Trinchero,[3] Alejandro F. Schinder,[3,4,*] Verónica C. Piatti,[3,4,*] and Emilio Kropff[2,4,5,*]
[1]Department of Physiology, Molecular and Cellular Biology Dr. Héctor Maldonado, Faculty of Exact and Natural Science, University of Buenos Aires, Buenos Aires C1428EGA, Argentina
[2]Laboratory of Physiology and Algorithms of the Brain, Leloir Institute (IIBBA-CONICET), Buenos Aires C1405BWE, Argentina
[3]Laboratory of Neuronal Plasticity, Leloir Institute (IIBBA-CONICET), Buenos Aires C1405BWE, Argentina
[4]These authors contributed equally
[5]Lead contact
*Correspondence: aschinder@leloir.org.ar (A.F.S.), vpiatti@leloir.org.ar (V.C.P.), ekropff@leloir.org.ar (E.K.)
https://doi.org/10.1016/j.celrep.2023.113086

SUMMARY

Mammalian hippocampal circuits undergo extensive remodeling through adult neurogenesis. While this process has been widely studied, the specific contribution of adult-born granule cells (aGCs) to spatial operations in the hippocampus remains unknown. Here, we show that optogenetic activation of 4-week-old (young) aGCs in free-foraging mice produces a non-reversible reconfiguration of spatial maps in proximal CA3 while rarely evoking neural activity. Stimulation of the same neuronal cohort on subsequent days recruits CA3 neurons with increased efficacy but fails to induce further remapping. In contrast, stimulation of 8-week-old (mature) aGCs can reliably activate CA3 cells but produces no alterations in spatial maps. Our results reveal a unique role of young aGCs in remodeling CA3 representations, a potential that can be depleted and is lost with maturation. This ability could contribute to generate orthogonalized downstream codes supporting pattern separation.

INTRODUCTION

Adult-born granule cells (aGCs) are added continuously to the dentate gyrus of the mammalian hippocampus, providing a unique source of plasticity absent in most other brain areas. In mice, development and maturation of aGCs takes about 8 weeks, at which time they are fully integrated to pre-existing circuits and display electrophysiological properties of perinatally born neurons.[1–6] By developmental week 4, aGCs go through a critical period in which they display enhanced levels of excitability and plasticity[7–9] and a low level of spatial information,[10,11] hinting at a distinctive computational role within the dentate gyrus function.[12,13] In agreement with this idea, immature aGCs have been shown to induce an increase in hippocampal sparsity in a short temporal window following their optogenetic stimulation.[11]

Behavioral experiments suggest that immature aGCs are involved in pattern separation, aiding their CA3 target circuits to form orthogonal representations for experiences that share a high degree of similarity.[14–22] In tasks that involve exploration, CA3 cells develop characteristic spatial maps that can be reorganized upon contextual changes, supporting the formation of distinctive representations.[23–27] Consistently, remapping decays along the proximodistal axis of CA3 in parallel to the relative prevalence of dentate vs. entorhinal inputs.[28–30] While converging evidence points to a critical role of immature aGCs in fine discrimination, the specific manner in which their distinctive properties influence representations in CA3 remains unknown.

RESULTS

To study the influence of aGCs on CA3 representations, we performed optogenetic stimulation of young (4-week-old) or mature (8-week-old) cohorts while recording neuronal activity in free-foraging $Ascl1^{CreERT2}$;$CAG^{floxStop-ChR2-EYFP}$ adult mice (Figures 1A–1C, S1A, and S1B). These mice expressed channelrhodopsin 2 (ChR2) in neural progenitor cells upon induction by tamoxifen.[31] Mice were then chronically implanted with optotrodes aimed at CA3. The level of expression of ChR2 and its efficacy for activating aGCs was similar in young and mature conditions (Figure S2). After 5 days of familiarization to free foraging in an open field arena, mice were exposed to multiple daily sessions over 4 days (Figure 1C; days 0–3), including 2 sessions in a novel environment (day 2). Square and circular arenas were used as familiar or novel environments in a counterbalanced way. By day 0, spatial representations were similar across sessions due to previous familiarization, while circuit properties such as average firing rate, spatial information, and stability showed no significant variations across conditions (Figures S1C, S3A, and S3B). From day 1 onward, young or mature aGCs were repeatedly stimulated during one intermediate session (Figure 1C, blue symbols) using 10 pulse trains (4 and 20 Hz), which reliably evoked spiking activity in some CA3 cells (Figure 1D).

To assess potential changes in spatial representation due to stimulation, we selected putative CA3 pyramidal cells that were active and stable on the first session of each day (Figure S1D). We first analyzed cells located in proximal CA3, comparing their

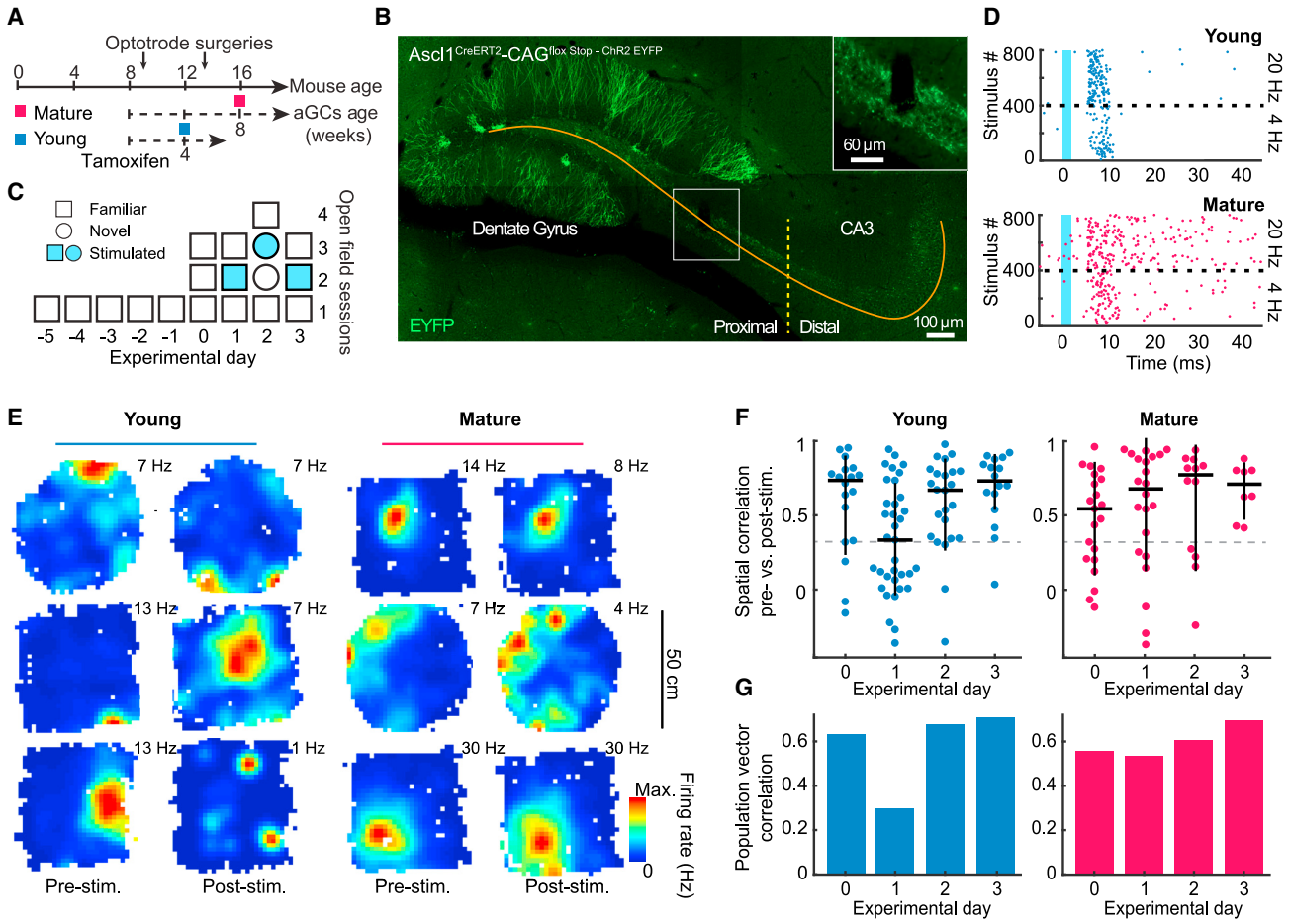

Figure 1. Remapping in CA3 induced by young aGC stimulation

(A) Schematics indicating tamoxifen injection and experimental sessions (colored squares) in mouse (top) and aGC cohort (bottom) timelines.

(B) Representative histology showing aGCs (EYFP, green), proximodistal axis (orange), and cutoff (yellow; 1,500 µm). Inset: tetrode tip.

(C) Behavioral sessions per experimental day in familiar or novel environments (shape code). Blue fill: stimulated session.

(D) Raster plots showing spiking of two CA3 cells evoked by young (top) or mature (bottom) aGC stimulation. Epochs of stimulation frequency indicated.

(E) Examples of spatial maps (color coded, maximum firing rate and session indicated) of CA3 cells (rows of subpanels) from day 1 in the young (left) and mature (right) conditions.

(F) Distribution (one circle per neuron; black: median and interquartile range [IQR]) of spatial correlation between pre- and post-stimulation maps in the young (left) and mature (right) conditions. Cells on each day, young: 18, 35, 24, and 16; mature: 21, 22, 11, and 8. Mice on each day, young: 7, 11, 8, and 5; mature: 6, 9, 4, and 4. Comparisons vs. day 0 (left-tailed Mann-Whitney test) for young condition day 1: $p = 0.01$; other days and conditions: $p > 0.25$.

(G) As (F) for population vector correlations. Comparisons vs. day 0 (shuffling) for young condition day 1: $p = 0.04$; other: $p > 0.4$.

See also Figures S1–S9.

spatial maps for the first (pre-stimulation) vs. last (post-stimulation) sessions through either spatial or population vector correlation (Figure S1E). Remarkably, substantial remapping was observed during day 1 in several cells following stimulation of young aCGs (Figures 1E, S1F, and S4–S6). In contrast, remapping was rare when optical stimulation targeted mature neurons, suggesting a specific role for immature aGCs in spatial processing. Across the cell population, spatial correlation was significantly lower on day 1 than on day 0 for the young condition, indicative of remapping, but was similar across days for the mature condition (Figures 1F, 1G, and S4C). An increase in locomotor activity in the post-stimulation session was also observed only in the young aGC condition (Figure S7A).

While average firing rate did not change across sessions, spiking activity transiently increased in spatial bins where young aGC stimulation had occurred, indicative of ongoing remodeling (Figures S7B–S7E). In contrast to what we observed in proximal CA3, cells located in distal CA3 did not exhibit significant remapping following stimulation of young or mature aGCs (Figures S8A and S8B). For this reason, we restricted further analyses to proximal CA3 representations.

Our findings suggest that remapping in CA3 might be induced by network remodeling triggered by the activity of young aGCs. We next asked if spatial representations could be further remodeled by reapplying the stimulation protocol on subsequent days. In contrast to the observations on day 1, maps for the familiar

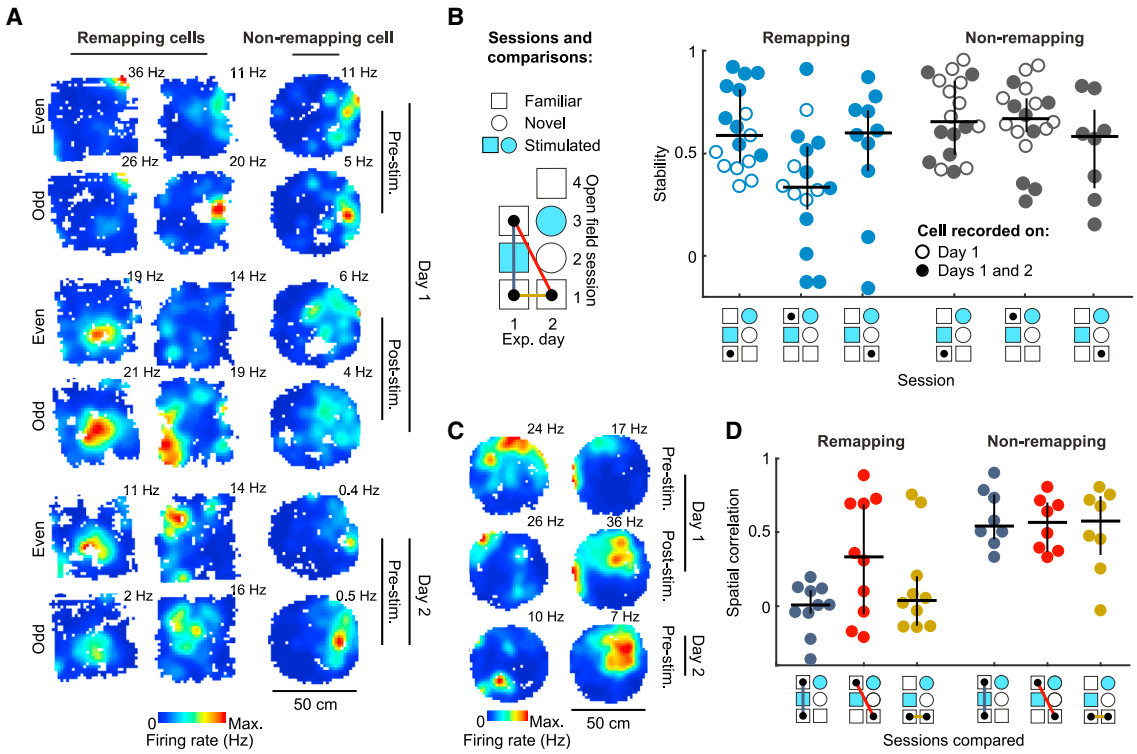

Figure 2. Destabilization and non-reversible remapping following the first stimulation of young aGCs

(A) Examples of stability for remapping (left) and non-remapping (right) CA3 cells (one per column). Spatial maps across sessions and days (color coded, maximum firing rate indicated) constructed with even (top) or odd (bottom) 30 s segments.

(B) Left: schematics of sessions and comparisons. Right: distribution across sessions (indicated graphically) of stability (one circle per neuron; black: median and IQR) for remapping (blue, n = 17) and non-remapping (gray; n = 18) cells recorded only on day 1 (hollow) or also on day 2 (filled). Left-tailed Wilcoxon tests between columns 1 vs. 2 (all circles): $p = 0.004$; 1 vs. 2 (filled circles): $p = 0.007$; 1 vs. 3 (filled circles): $p = 0.07$; similar comparisons for non-remapping cells: $p > 0.15$. Left-tailed Mann-Whitney test between columns 1 vs. 4 (all circles): $p = 0.4$.

(C) Examples of spatial maps (color coded, maximum firing rate indicated) of remapping cells (columns) across days and sessions.

(D) Distribution of spatial correlation between maps of indicated sessions (color coded as in B; one circle per neuron; black: median and IQR) for remapping (left; n = 10) and non-remapping (right; n = 8) cells. Right-tailed Wilcoxon test against zero-median hypothesis for remapping cells from left to right: $p = 0.46$, 0.02, and 0.24; for non-remapping cells: $p < 0.02$.

See also Figure S3.

environment remained unchanged after stimulation in a novel arena (day 2) or in the same arena (day 3; Figures 1F and 1G). These results point to a fast depletion in the capacity of young aGCs to induce remapping.

Mice in the mature condition (16 weeks old) were older than those in the young condition (12 weeks old). To rule out the possibility that remapping was related to mouse, rather than neuronal, age, we stimulated a mature cohort in a group of younger mice (12 weeks old). We found no changes in spatial maps, pointing to neuronal age as the critical factor behind remapping (Figure S9).

Our results reveal a unique potential for young aGCs to induce remapping in proximal CA3 spatial representations. This ability extinguishes once deployed and is lost with neuronal maturation.

To characterize the remodeling of CA3 spatial representations triggered by the activation of aGCs, we classified cells recorded on day 1 in the young condition into remapping and non-remapping subpopulations, according to the degree of correlation between their firing maps before and after stimulation (Figures 1F and S1E). Using this classification, we assessed whether remapping was associated with changes in the stability of spatial maps. Stability was defined as the spatial correlation between maps constructed with data from even vs. odd segments after dividing each session into consecutive 30 s windows. Remapping and non-remapping cells displayed similar levels of stability before the stimulation session. However, while non-remapping cells continued to display high stability, remapping cells showed a marked reduction in stability after stimulation (Figures 2A, 2B, and S3C–S3E).

To characterize the time course of this process, we monitored remapping cells on the following day and found that stability was recovered by the first session of day 2 (Figure 2B). This recovery could indicate that remapping cells returned to pre-stimulation maps or acquired new stable maps. To distinguish between these alternatives, we analyzed the correlation between maps corresponding to different sessions of days 1 and 2 (Figures 2C and 2D). Pre-stimulation maps on day 2 were different from pre-stimulation maps on day 1 but preserved post-stimulation features. This result supports the idea that stimulation triggers the formation

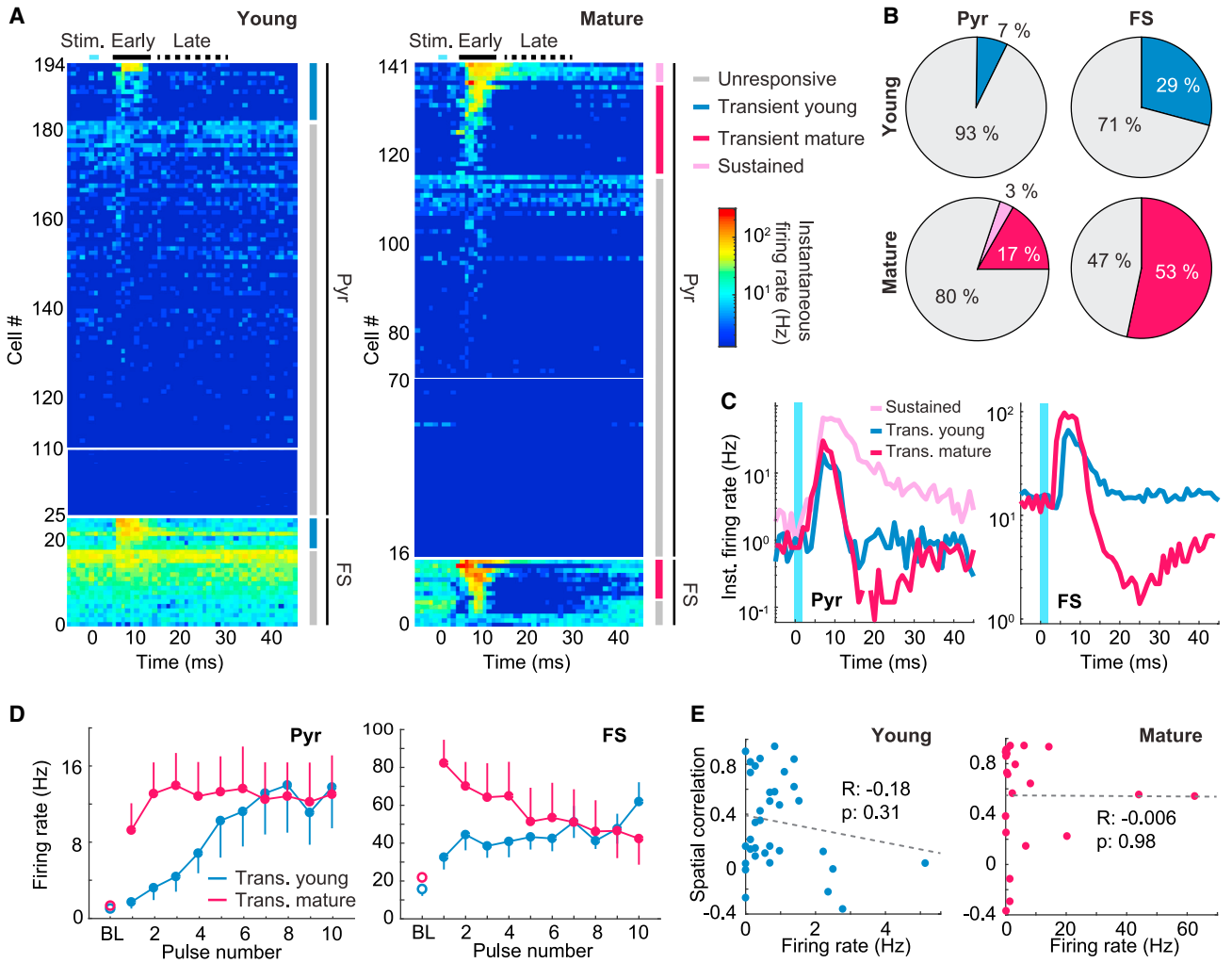

Figure 3. Evoked activity patterns in CA3 are not related to remapping

(A) Activity (color coded) relative to aGC stimulation in the young (left) or mature (right) condition for all recorded cells (rows), averaged across all stimulation pulses. Cells are ordered according to strength of response, putative cell type, and response pattern (indicated). Stimulation, early, and late windows are indicated. Note compression for silent cells (young: 25–109, mature: 16–69). Pyr, transient: 13/170 (young) and 21/126 (mature); sustained: 5/126. FS, transient: 7/24 (young) and 8/15 (mature).

(B) Distribution of response patterns (color coded as in A) for Pyr (left) and FS (right) in the young (top) and mature (bottom) conditions. Comparisons of transient cell recruitment in young vs. mature condition (shuffling): p = 0.004 (Pyr) and 0.06 (FS).

(C) Mean response patterns (color coded) for Pyr (left) or FS (right) cells. Comparisons of transient cell response between conditions (shuffling) for early window: p = 0.46 (Pyr) and 0.1 (FS); for late window: p = 0.03 (Pyr) and 0.007 (FS). Comparisons of transient (mature) vs. sustained response (shuffling): p = 0.002 (early window) and p < 0.0001 (late window).

(D) Evoked activity of transient Pyr (left) or FS (right) cells along 10 pulse stimulation trains (mean ± SEM; BL, baseline). Comparison of ratio between last and first pulse vs. 1 (two-tailed Wilcoxon test): Pyr p = 0.0002 (young; n = 13) and 0.02 (mature; n = 21); FS p = 0.06 (young; n = 7) and 0.2 (mature; n = 8).

(E) Spatial correlation (Figure 1F) vs. early evoked activity on day 1 in young (left) and mature (right) conditions (regression coefficients indicated).

See also Figures S8 and S10–S13.

of new maps. Non-remapping cells, in contrast, maintained their maps throughout sessions and days.

Collectively, these results demonstrate that the stimulation of young aGCs elicits a transient loss of stability in spatial maps that is recovered within 24 h. Remapping CA3 cells ultimately form new stable maps that are uncorrelated with the original ones.

We next characterized CA3 spiking activity evoked by the same optogenetic stimulation. We visualized evoked activity of all recorded cells aligned to the stimulus onset and averaged across all stimulation pulses for young or mature aGCs (Figures 3A and S10). Stimulation typically evoked an increase in firing rate during an early window (5–13 ms post-stimulus), followed by a return to baseline values or brief inhibition during a late window (15–30 ms; Figure S11A). These features were found in both putative pyramidal (Pyr) and fast spiking (FS) cells, defined according to their mean firing rate.

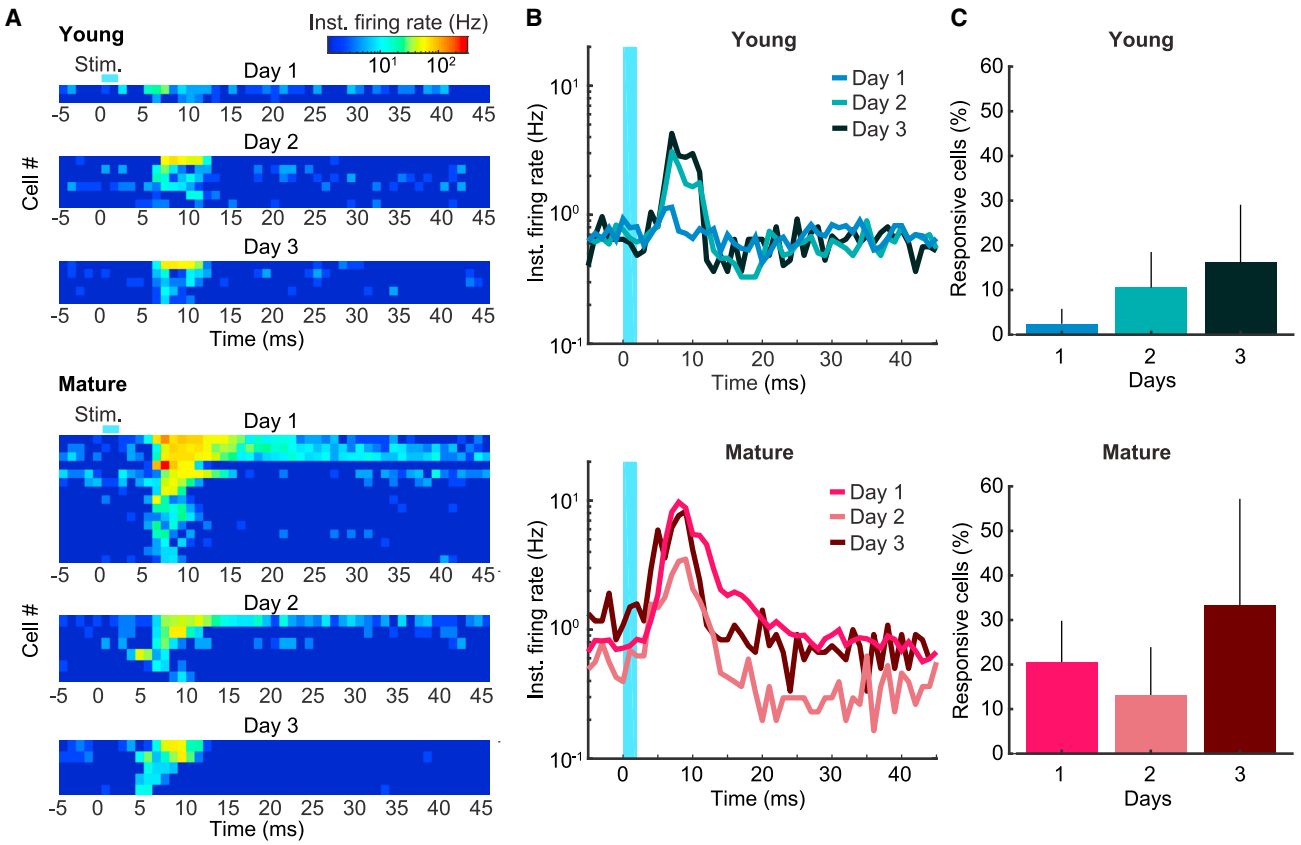

Figure 4. Sharp increase in CA3 recruitment following the first stimulation of young aGCs

(A) Evoked activity heatmaps for all responsive Pyr cells (rows) across days (subpanels) in the young (top, 13 cells) or mature (bottom, 26 cells) conditions.

(B) Evoked activity averaged over all recorded Pyr cells across days (color coded) in the young (top; n = 82, 57, and 31) and mature (bottom; n = 73, 38, and 15) conditions. Comparisons of early response in the young condition (shuffling): p = 0.04 (days 1 vs. 2) and 0.03 (days 1 vs. 3). Similar comparisons in the mature condition: p > 0.1.

(C) Percentage of responsive Pyr across days in the young (top; n = 2/82, 6/57, and 5/31) and mature (bottom; n = 15/73, 6/38, and 5/15) conditions. Kruskal-Wallis tests: young p = 0.03; mature p = 0.25. Dunn's post hoc tests for the young condition: p = 0.08 (days 1 vs. 2) and 0.02 (days 1 vs. 3).

See also Figure S8.

We classified cell responses using a generalized linear model that compared activity during the early and late windows with a pre-stimulus baseline. In general, cells were classified as either "transient" (early response) or "non-responsive." Mature aGCs recruited a higher proportion of transient cells than young aGCs, and responses were followed by a strong inhibition (Figures 3B, 3C, S8C–S8E, and S11B–S11D). However, the amplitude of individual transient responses in both conditions was similar. In the mature condition, we found a small additional group of Pyr cells classified as "sustained" that exhibited a remarkably strong initial response that remained elevated throughout the late window.

We also analyzed short-term plasticity of evoked spiking responses. For Pyr cells, pulse trains delivered to young aGCs elicited small initial responses with remarkable facilitation of post-synaptic spiking along subsequent pulses (about 6-fold; Figures 3D, S8F, S11E, S12, and S13). In contrast, stimulation of mature aGCs elicited a strong initial response with less facilitation (transient: 1.5-fold; sustained: 3-fold). In FS cells, responses to stimulation of young aGCs were somewhat facilitated, while activity elicited by mature aGCs exhibited depression. These results reveal distinct features of synaptic transmission and plasticity during neuronal maturation and provide *in vivo* evidence that aGCs continue to develop their connections beyond 4 weeks of age.

We next asked if there was a relationship between the remapping observed on day 1 (Figures 1F and 1G) and the efficacy of evoked activity. Responses elicited by young aGC stimulation were low and similar for remapping and non-remapping cells (Figure S11F). Furthermore, we found no correlation between evoked activity and remapping across the Pyr population (Figures 3E and S11G). While remapping was not predicted by the behavior of individual CA3 cells, it was associated with prominent modifications at the network level. Compared to day 1, overall activity evoked by young aGCs changed substantially on subsequent days, resulting in a several-fold increase in the recruitment of Pyr cells (Figures 4, S8G, and S8H). In contrast, the proportion of recruited Pyr cells in the mature condition was initially high and displayed no significant changes across days. The large increase in post-synaptic responsiveness in the young condition suggests that substantial synaptic and network remodeling took place following the first stimulation of aGCs.

DISCUSSION

Our results demonstrate that stimulation of a small number of inputs from young aGCs triggers extensive network modifications. These changes are initially visualized at the level of spatial code as a destabilization and reorganization of CA3 maps. Within 24 h, post-synaptic recruitment increases several fold, and cells form new stable representations of the environment, while aGCs lose their potential to induce further changes. Remapping is an indication that young aGCs trigger activity-dependent remodeling of the post-synaptic circuits, a process that might be enabled by the enhanced excitability and synaptic plasticity displayed by young aGCs.[3,7–9,32,33] In line with this hypothesis, a recent study found that exercise, a natural booster of adult neurogenesis, increased CA1 spatial representation drift throughout days.[34] In contrast, stimulation of mature aGCs recruits a higher proportion of CA3 principal cells but does not produce remapping, consistent with previous observations.[35,36]

During the first stimulation session of young aGCs, evoked activity in CA3 Pyr cells was very low. This result is compatible with previous reports of an increase in hippocampal sparseness triggered by the optogenetic stimulation of young aGCs.[11] Our results, however, indicate that activity evoked within the ms range after each stimulation is not directly related to remapping, which takes place at a longer timescale (minutes to hours). A similar dissociation between evoked activity and remapping was described in previous studies showing that reorganization of hippocampal place fields can occur away from the stimulation site or in non-responsive neurons.[37–39] As discussed in these studies, subthreshold mechanisms could be a potential candidate to explain the lack of correlation we found between post-synaptic spiking activity and remodeling.

The dynamic role played by young aGCs potentially explains why remapping in CA3 may not require massive differences in population coding one synapse upstream.[23–25,40–46] Instead, we speculate that young aGCs could be specifically recruited by experiences involving novelty or surprise,[10] which would lead to the formation of new orthogonal CA3 codes to represent them, thus promoting pattern separation.[12,13,17,18,20,21] The transient capacity for remapping would tie experience-driven demand for novel CA3 representations to the continuous supply of new neurons as an irreplaceable source of hippocampal plasticity.

Limitations of the study

First, we used classic optogenetic tools to study the influence of aGCs on CA3 spatial representations. Gain-of-function methods, such as those employed here, are powerful tools that have been widely employed in neuroscience for almost two decades.[47] However, increasing the activity of an entire cohort of aGCs by applying several hundreds of light pulses may not accurately represent the spiking patterns that occur under physiological conditions in the aGC-CA3 synapse. To ameliorate this distortive methodological effect, the stimulation patterns we used were chosen based on previous studies that either optogenetically manipulated dentate gyrus (DG) cells[3,11,35,36,48,49] or studied their activity under circumstances that were closer to those naturally occurring.[50] Therefore, we do not claim to prove that aGCs are naturally activated and consequently produce remapping in CA3, but we provide evidence that these adult-born neurons have the potential to induce remapping in CA3. This potential is lost with maturation and could be key to understanding hippocampal neurogenic function.

Second, the DG was proposed as the main candidate for the implementation of pattern separation.[13] Several studies have associated the daily addition of new neurons in the DG to this function.[1,10,12,14,18,19,21] Given that remapping is thought to reflect pattern separation, at least under certain circumstances,[24–26] our results suggest that the potential of young aGCs to reorganize CA3 spatial maps could mediate its implementation in the DG-CA3 network.[41] However, our behavioral procedures were not designed to require DG-mediated pattern separation. Hence, our claims relate to the plasticity of hippocampal spatial representations in general.

Third, we found no direct relationship between the activity evoked in CA3 by young aGCs and remapping on day 1. Studies in other subfields of the hippocampus have suggested that spatial map reorganization is triggered by post-synaptic subthreshold mechanisms.[37–39] Our study is limited by the technique of extracellular electrophysiology, which only provides information about spiking activity. Thus, the potential effects of our optogenetic manipulation due to post-synaptic subthreshold mechanisms could not be assessed. However, we found a several-fold increase in spiking recruitment across days in the young condition, which was inversely related to the occurrence of remapping, hinting toward the mediation of such a mechanism.

STAR★METHODS

Detailed methods are provided in the online version of this paper and include the following:

- KEY RESOURCES TABLE
- RESOURCE AVAILABILITY
  - Lead contact
  - Materials availability
  - Data and code availability
- EXPERIMENTAL MODEL AND STUDY PARTICIPANT DETAILS
  - Animals
- METHOD DETAILS
  - Experimental groups
  - TAM induction
  - Opto-drives
  - Surgery
  - Lowering of tetrodes
  - Behavior
  - Optical stimulation
  - Data collection
  - Spike sorting
  - Brain processing for histology
  - Count of ChR2 expressing cells
  - *Ex vivo* electrophysiology recordings
- QUANTIFICATION AND STATISTICAL ANALYSIS
  - Spatial maps
  - Characterization of firing rate variation in stimulated bins

- Shuffling statistics
- Statistical analysis
- Classification of patters of evoked activity
- Light-pulse train analysis
- Cell selection criteria

SUPPLEMENTAL INFORMATION

Supplemental information can be found online at https://doi.org/10.1016/j.celrep.2023.113086.

ACKNOWLEDGMENTS

We thank the members of the E.K. and A.F.S. labs for insightful discussions, as well as the Service of Microscopy and Images of the Leloir Institute Foundation. A.F.S., E.K., M.F.T., and V.C.P. are investigators in the Consejo Nacional de Investigaciones Científicas y Técnicas. M.M. was supported by a CONICET fellowship. This work was supported by grants from the National Institute of Neurological Disorders and Stroke (NINDS) and the Fogarty International Center (FIC) (R01NS103758) to A.F.S.; the Argentine Agency for the Promotion of Science and Technology (PICT-2016-3611), the Pew Latin American Fellows Program in the Biomedical Sciences, and the Bunge & Born Foundation/Williams Foundation/The Pew Charitable Trusts Repatriation Grants to V.C.P.; and the Argentine Agency for the Promotion of Science and Technology (PICT 2019-2596) and the Human Frontier Science Program (HFSP-RGY0072/2018) to E.K.

AUTHOR CONTRIBUTIONS

Conceptualization, M.M., E.K., V.C.P., and A.F.S.; methodology, M.M. and V.C.P.; validation, M.M., M.F.T., E.K., and V.C.P.; resources, E.K., V.C.P., and A.F.S.; formal analysis, M.M., E.K., and M.F.T.; investigation, M.M. and M.F.T.; data curation, M.M.; visualization, M.M. and M.F.T.; writing – original draft, M.M. and E.K.; writing – review & editing, M.M., M.F.T., E.K., V.C.P., and A.F.S.; supervision, E.K., V.C.P., and A.F.S.; project administration, E.K. and V.C.P.; funding acquisition, E.K., V.C.P., and A.F.S.

DECLARATION OF INTERESTS

The authors declare no competing interests.

Received: March 15, 2023
Revised: May 30, 2023
Accepted: August 15, 2023
Published: September 6, 2023

REFERENCES

1. Bonaguidi, M.A., Song, J., Ming, G.-l., and Song, H. (2012). A unifying hypothesis on mammalian neural stem cell properties in the adult hippocampus. Curr. Opin. Neurobiol. *22*, 754–761.
2. Groisman, A.I., Yang, S.M., and Schinder, A.F. (2020). Differential coupling of adult-born granule cells to parvalbumin and somatostatin interneurons. Cell Rep. *30*, 202–214.e4.
3. Gu, Y., Arruda-Carvalho, M., Wang, J., Janoschka, S.R., Josselyn, S.A., Frankland, P.W., and Ge, S. (2012). Optical controlling reveals time-dependent roles for adult-born dentate granule cells. Nat. Neurosci. *15*, 1700–1706.
4. Laplagne, D.A., Espósito, M.S., Piatti, V.C., Morgenstern, N.A., Zhao, C., van Praag, H., Gage, F.H., and Schinder, A.F. (2006). Functional convergence of neurons generated in the developing and adult hippocampus. PLoS Biol. *4*, e409.
5. Temprana, S.G., Mongiat, L.A., Yang, S.M., Trinchero, M.F., Alvarez, D.D., Kropff, E., Giacomini, D., Beltramone, N., Lanuza, G.M., and Schinder, A.F. (2015). Delayed coupling to feedback inhibition during a critical period for the integration of adult-born granule cells. Neuron *85*, 116–130.
6. Zhao, C., Deng, W., and Gage, F.H. (2008). Mechanisms and functional implications of adult neurogenesis. Cell *132*, 645–660.
7. Ge, S., Yang, C.-h., Hsu, K.-s., Ming, G.-l., and Song, H. (2007). A critical period for enhanced synaptic plasticity in newly generated neurons of the adult brain. Neuron *54*, 559–566.
8. Marín-Burgin, A., Mongiat, L.A., Pardi, M.B., and Schinder, A.F. (2012). Unique processing during a period of high excitation/inhibition balance in adult-born neurons. Science *335*, 1238–1242.
9. Schmidt-Hieber, C., Jonas, P., and Bischofberger, J. (2004). Enhanced synaptic plasticity in newly generated granule cells of the adult hippocampus. Nature *429*, 184–187.
10. Danielson, N.B., Kaifosh, P., Zaremba, J.D., Lovett-Barron, M., Tsai, J., Denny, C.A., Balough, E.M., Goldberg, A.R., Drew, L.J., Hen, R., et al. (2016). Distinct contribution of adult-born hippocampal granule cells to context encoding. Neuron *90*, 101–112.
11. McHugh, S.B., Lopes-dos-Santos, V., Gava, G.P., Hartwich, K., Tam, S.K.E., Bannerman, D.M., and Dupret, D. (2022). Adult-born dentate granule cells promote hippocampal population sparsity. Nat. Neurosci. *25*, 1481–1491.
12. Kropff, E., Yang, S.M., and Schinder, A.F. (2015). Dynamic role of adult-born dentate granule cells in memory processing. Curr. Opin. Neurobiol. *35*, 21–26.
13. Treves, A., Tashiro, A., Witter, M.P., and Moser, E.I. (2008). What is the mammalian dentate gyrus good for? Neuroscience *154*, 1155–1172.
14. Clelland, C.D., Choi, M., Romberg, C., Clemenson, G.D., Jr., Fragniere, A., Tyers, P., Jessberger, S., Saksida, L.M., Barker, R.A., Gage, F.H., and Bussey, T.J. (2009). A functional role for adult hippocampal neurogenesis in spatial pattern separation. Science *325*, 210–213.
15. Goodrich-Hunsaker, N.J., Hunsaker, M.R., and Kesner, R.P. (2008). The interactions and dissociations of the dorsal hippocampus subregions: how the dentate gyrus, CA3, and CA1 process spatial information. Behav. Neurosci. *122*, 16–26.
16. Lee, I., and Kesner, R.P. (2004). Differential contributions of dorsal hippocampal subregions to memory acquisition and retrieval in contextual fear-conditioning. Hippocampus *14*, 301–310.
17. Luna, V.M., Anacker, C., Burghardt, N.S., Khandaker, H., Andreu, V., Millette, A., Leary, P., Ravenelle, R., Jimenez, J.C., Mastrodonato, A., et al. (2019). Adult-born hippocampal neurons bidirectionally modulate entorhinal inputs into the dentate gyrus. Science *364*, 578–583.
18. Nakashiba, T., Cushman, J.D., Pelkey, K.A., Renaudineau, S., Buhl, D.L., McHugh, T.J., Rodriguez Barrera, V., Chittajallu, R., Iwamoto, K.S., McBain, C.J., et al. (2012). Young dentate granule cells mediate pattern separation, whereas old granule cells facilitate pattern completion. Cell *149*, 188–201.
19. Piatti, V.C., Ewell, L.A., and Leutgeb, J.K. (2013). Neurogenesis in the dentate gyrus: carrying the message or dictating the tone. Front. Neurosci. *7*, 50.
20. Scobie, K.N., Hall, B.J., Wilke, S.A., Klemenhagen, K.C., Fujii-Kuriyama, Y., Ghosh, A., Hen, R., and Sahay, A. (2009). Krüppel-like factor 9 is necessary for late-phase neuronal maturation in the developing dentate gyrus and during adult hippocampal neurogenesis. J. Neurosci. *29*, 9875–9887.
21. Tronel, S., Belnoue, L., Grosjean, N., Revest, J.M., Piazza, P.V., Koehl, M., and Abrous, D.N. (2012). Adult-born neurons are necessary for extended contextual discrimination. Hippocampus *22*, 292–298.
22. Yassa, M.A., and Stark, C.E.L. (2011). Pattern separation in the hippocampus. Trends Neurosci. *34*, 515–525.
23. Hainmueller, T., and Bartos, M. (2020). Dentate gyrus circuits for encoding, retrieval and discrimination of episodic memories. Nat. Rev. Neurosci. *21*, 153–168.

24. Knierim, J.J., and Neunuebel, J.P. (2016). Tracking the flow of hippocampal computation: Pattern separation, pattern completion, and attractor dynamics. Neurobiol. Learn. Mem. *129*, 38–49.

25. Leutgeb, J.K., Leutgeb, S., Moser, M.-B., and Moser, E.I. (2007). Pattern separation in the dentate gyrus and CA3 of the hippocampus. science *315*, 961–966.

26. Moser, E.I., Kropff, E., and Moser, M.-B. (2008). Place cells, grid cells, and the brain's spatial representation system. Annu. Rev. Neurosci. *31*, 69–89.

27. van Dijk, M.T., and Fenton, A.A. (2018). On how the dentate gyrus contributes to memory discrimination. Neuron *98*, 832–845.e5.

28. Lee, H., Wang, C., Deshmukh, S.S., and Knierim, J.J. (2015). Neural population evidence of functional heterogeneity along the CA3 transverse axis: pattern completion versus pattern separation. Neuron *87*, 1093–1105.

29. Lu, L., Igarashi, K.M., Witter, M.P., Moser, E.I., and Moser, M.-B. (2015). Topography of place maps along the CA3-to-CA2 axis of the hippocampus. Neuron *87*, 1078–1092.

30. Witter, M.P. (2007). Intrinsic and extrinsic wiring of CA3: indications for connectional heterogeneity. Learn. Mem. *14*, 705–713.

31. Yang, S.M., Alvarez, D.D., and Schinder, A.F. (2015). Reliable genetic labeling of adult-born dentate granule cells using Ascl1CreERT2 and GlastCreERT2 murine lines. J. Neurosci. *35*, 15379–15390.

32. Toni, N., Laplagne, D.A., Zhao, C., Lombardi, G., Ribak, C.E., Gage, F.H., and Schinder, A.F. (2008). Neurons born in the adult dentate gyrus form functional synapses with target cells. Nat. Neurosci. *11*, 901–907.

33. Toni, N., Teng, E.M., Bushong, E.A., Aimone, J.B., Zhao, C., Consiglio, A., van Praag, H., Martone, M.E., Ellisman, M.H., and Gage, F.H. (2007). Synapse formation on neurons born in the adult hippocampus. Nat. Neurosci. *10*, 727–734.

34. de Snoo, M.L., Miller, A.M.P., Ramsaran, A.I., Josselyn, S.A., and Frankland, P.W. (2023). Exercise accelerates place cell representational drift. Curr. Biol. *33*, R96–R97.

35. Lee, J., Yun, M., Cho, E., Lee, J.W., Lee, D., and Jung, M.W. (2019). Transient effect of mossy fiber stimulation on spatial firing of CA3 neurons. Hippocampus *29*, 639–651.

36. Restivo, L., Niibori, Y., Mercaldo, V., Josselyn, S.A., and Frankland, P.W. (2015). Development of adult-generated cell connectivity with excitatory and inhibitory cell populations in the hippocampus. J. Neurosci. *35*, 10600–10612.

37. Dragoi, G., Harris, K.D., and Buzsáki, G. (2003). Place representation within hippocampal networks is modified by long-term potentiation. Neuron *39*, 843–853.

38. McKenzie, S., Huszár, R., English, D.F., Kim, K., Christensen, F., Yoon, E., and Buzsáki, G. (2021). Preexisting hippocampal network dynamics constrain optogenetically induced place fields. Neuron *109*, 1040–1054.e7.

39. Rickgauer, J.P., Deisseroth, K., and Tank, D.W. (2014). Simultaneous cellular-resolution optical perturbation and imaging of place cell firing fields. Nat. Neurosci. *17*, 1816–1824.

40. GoodSmith, D., Chen, X., Wang, C., Kim, S.H., Song, H., Burgalossi, A., Christian, K.M., and Knierim, J.J. (2017). Spatial representations of granule cells and mossy cells of the dentate gyrus. Neuron *93*, 677–690.e5.

41. GoodSmith, D., Lee, H., Neunuebel, J.P., Song, H., and Knierim, J.J. (2019). Dentate gyrus mossy cells share a role in pattern separation with dentate granule cells and proximal CA3 pyramidal cells. J. Neurosci. *39*, 9570–9584.

42. Hainmueller, T., and Bartos, M. (2018). Parallel emergence of stable and dynamic memory engrams in the hippocampus. Nature *558*, 292–296.

43. Kanter, B.R., Lykken, C.M., Avesar, D., Weible, A., Dickinson, J., Dunn, B., Borgesius, N.Z., Roudi, Y., and Kentros, C.G. (2017). A novel mechanism for the grid-to-place cell transformation revealed by transgenic depolarization of medial entorhinal cortex layer II. Neuron *93*, 1480–1492.e6.

44. Miao, C., Cao, Q., Ito, H.T., Yamahachi, H., Witter, M.P., Moser, M.-B., and Moser, E.I. (2015). Hippocampal remapping after partial inactivation of the medial entorhinal cortex. Neuron *88*, 590–603.

45. Schlesiger, M.I., Boublil, B.L., Hales, J.B., Leutgeb, J.K., and Leutgeb, S. (2018). Hippocampal global remapping can occur without input from the medial entorhinal cortex. Cell Rep. *22*, 3152–3159.

46. Senzai, Y., and Buzsáki, G. (2017). Physiological properties and behavioral correlates of hippocampal granule cells and mossy cells. Neuron *93*, 691–704.e5.

47. Deisseroth, K. (2015). Optogenetics: 10 years of microbial opsins in neuroscience. Nat. Neurosci. *18*, 1213–1225.

48. Guo, N., Soden, M.E., Herber, C., Kim, M.T., Besnard, A., Lin, P., Ma, X., Cepko, C.L., Zweifel, L.S., and Sahay, A. (2018). Dentate granule cell recruitment of feedforward inhibition governs engram maintenance and remote memory generalization. Nat. Med. *24*, 438–449.

49. Liu, X., Ramirez, S., Pang, P.T., Puryear, C.B., Govindarajan, A., Deisseroth, K., and Tonegawa, S. (2012). Optogenetic stimulation of a hippocampal engram activates fear memory recall. Nature *484*, 381–385.

50. Henze, D.A., Wittner, L., and Buzsáki, G. (2002). Single granule cells reliably discharge targets in the hippocampal CA3 network in vivo. Nat. Neurosci. *5*, 790–795.

STAR★METHODS

KEY RESOURCES TABLE

REAGENT or RESOURCE	SOURCE	IDENTIFIER
Antibodies		
Anti GFP (chicken polyclonal)	Aves Labs Inc.	Cat# GFP-1020; RRID:AB_10000240
Donkey anti-chicken Cy2	Jackson ImmunoResearch Laboratories	Cat# 703-225-155; RRID:AB_2340370
Chemicals, peptides, and recombinant proteins		
Kynurenic acid	MP Biomedicals	Cat# K3375
Experimental models: Organisms/strains		
Ascl1$^{tm1(Cre/ERT2)Jejo}$/J	The Jackson Laboratory	MGI: 4452601
CAG$^{floxStopChR2-EYFP}$ (Ai32)Gt(ROSA) 26Sor$^{tm32CAGCOP4*H134R/EYFP)Hze}$/J)	The Jackson Laboratory	MGI: 5577173
C57BL/6 mice	Leloir Institute Facility	N/A
Software and algorithms		
LSM 5 Pascal v. 3.2 SP2	Zeiss	https://www.zeiss.com/
Clampfit 10.6	Molecular Devices	https://www.moleculardevices.com/
Zen blue	Zeiss	https://www.zeiss.com/
MATLAB 2017a	MathWorks	https://www.mathworks.com/
Cheetah	Neuralynx Inc.	https://neuralynx.com/
Nano Z	White Matter	https://white-matter.com/

RESOURCE AVAILABILITY

Lead contact

Further information and requests for resources should be directed to and will be fulfilled by the lead contact, Emilio Kropff (ekropff@leloir.org.ar).

Materials availability

This study did not generate new unique reagents.

Data and code availability

- All data reported in this paper will be shared by the lead contact upon request.
- This paper does not report original code.
- Any additional information required to reanalyze the data reported in this paper is available from the lead contact upon request.

EXPERIMENTAL MODEL AND STUDY PARTICIPANT DETAILS

Animals

Experimental protocols were approved by the Institutional Animal Care and Use Committee of the Leloir Institute, Protocol No. 83 according to the Principles for Biomedical Research involving animals of the Council for International Organizations for Medical Sciences and provisions stated in the Guide for the Care and Use of Laboratory Animals.

Twenty-seven Ascl1^{CreERT2} – CAG $^{flox\ Stop\ -\ ChR2\ EYFP}$ mice (12 male and 15 female) were housed at 2–4 mice per cage from weaning. Three days before tamoxifen (TAM) injection they were transferred to individual cages, where they stayed until the end of the experiments. A running wheel was included in these cages. Animals were maintained on an inverted 12-h light/12-h schedule (lights on 08:00 p.m.) and tested in the dark phase. Water and food were provided *ad libitum* throughout the experiments.

A different set of 8 Ascl1^{CreERT2} – CAG $^{flox\ Stop\ -\ ChR2\ EYFP}$ mice (3 male and 5 female) was used to compare aGC counts across conditions (see section Count of ChR2 expressing cells; Figures S2A and S2B). In addition, another group of 10 Ascl1^{CreERT2} – CAG $^{flox\ Stop\ -\ ChR2\ EYFP}$ mice (6 male and 4 female) were used in *ex vivo* electrophysiology recordings to compare ChR2 efficacy across conditions (see *Ex vivo* electrophysiology recordings section; Figures S2C–S2E).

METHOD DETAILS

Experimental groups

Experimental conditions were defined by the age of the aGC cohort expressing ChR2. In the young and mature conditions, the expression was induced by TAM injections when animals were 8 weeks old. Experiments in the young condition (6 male and 6 female) were performed 4 weeks later and in the mature condition (7 male and 5 female) 8 weeks later.

In a control condition (2 male and 5 female), aimed to test mature aGCs in 12-week-old animals, TAM was injected when animals were 4 weeks old and experiments were done 8 weeks later.

TAM induction

TAM was delivered intraperitoneally at 120 μg/g/injection through four injections in 2 consecutive days (early morning and late afternoon) to achieve indelible expression of ChR2-EYFP in aGCs (Figures 1A, S1B and S2A). The wheel-to-TAM period was aimed to maximize the number of labeled neurons expressing ChR2-EYFP (Yang et al., 2015).

Opto-drives

Tetrodes (~25-μm in diameter) were constructed from four strands of tungsten wire (99.95% tungsten, 12.5 μm in diameter, California Fine Wire Company, USA), bound together by twisting and melting their insulation with hot air (approximately 110°C). Five tetrodes were loaded and glued into a nested assembly of stainless-steel tubes and mounted into the microdrive (Axona Limited, UK), (total weight around 2.5 g). One of the tetrodes was coupled to an optic fiber (250 μm diameter) with its tip traveling 500–700 μm below the optic fibers end. Since all the tetrodes were aimed to CA3, the optic fiber stimulated aGC axons. The tetrodes excited the microdrive through a guide cannula in an approximately rectangular arrangement (approximate spacing 400-μm) and every tetrode could be moved independently via a drive screw (160 μm per turn). Each tetrode was cut flat and its tip was gold-plated (gold plating solution, Neuralynx, MT, USA) to reduce the 1 kHz impedance of individual wires to 0.2–0.4 MΩ (Nano Z, White Matter, WA, USA).

Surgery

The surgeries to chronically implant opto-drives were performed 4 days or 32 days after TAM induction. This procedure was conducted under ketamine-xylazine anesthesia (150 μg ketamine/15 μg xylazine in 10 μL saline/g). A circular opening (approximately 1 mm in diameter) was made in the skull above the right dorsal hippocampus. The center of the craniotomy was 2.4 mm lateral to the midline and 1.7 mm posterior to bregma. Next, 7 jeweler's screws were inserted in holes drilled in the skull around the craniotomy. After the removal of the dura, the tetrode tips were lowered 1 mm below the brain surface. The craniotomy was filled with a biocompatible transparent gel Neuroseal obtained by combining equal parts of 0.5% sodium alginate and 10% calcium chloride, both previously dissolved in distilled water and stored separately. The skull, the screws and the base of the opto-microdrives were then covered with auto-crystal acrylic, dental cement. After surgery animals were left to recover for 3–5 days.

Lowering of tetrodes

During a period of 2–3 weeks after recovery from surgery, tetrodes were progressively lowered toward the CA3 pyramidal layer. One of the tetrodes served as a reference and was left in an electrically-quiet zone above the hippocampus. This reference tetrode was used for differential recordings. The remaining four tetrodes served as recording probes. CA1 sharp-wave-ripple complexes and soma layer activity, visualized with Cheetah (Neuralynx, Inc., MT, USA), were the main guides to position the electrodes on the CA3 pyramidal cell layer.

Behavior

Free-foraging experiments were conducted in two open field (OF) arenas: a 46 cm side square and a 50 cm diameter circle (Figures 1A and S9). Arena walls were made out of acrylic (circle) or contact paper covered cardboard (square) and acrylic floors. A white (square) or orange (circle) card (20 × 25 cm) was placed as a local cue in the south wall to facilitate orientation. Since no curtains were used, objects in the room provided additional distal cues. In sessions 2 and 3 of day 2, a novel OF was positioned in the same experimental room approximately 1.5 m away from the position of the familiar environment and the local cue card was placed in the east wall. Square and circle arenas were used as familiar or novel environments in a counterbalanced way.

A group of 4 mice (3 males and 1 female) belonging to the young condition were not sacrificed immediately after the last day of experimentation. Instead, they were kept in their home cage for around 3 weeks to repeat the battery of experiments with the same aGC cohort, this time in the mature condition. In this second round of experiments, animals were already familiarized with the square and circle environments. Thus, while the familiar environment was the same as in the first round of experiments, the novel environment was a 45 cm side equilateral triangle with contact paper cardboard walls and acrylic floor. Differences between data collected during this second round of experiments and the one collected from animals in the regular mature condition (aGCs stimulated for the first time at 8 weeks old; 4 male and 4 female) were assessed. Despite the fact that these 5 mice had additional experience with experimenter manipulations and free-foraging in the OF, and that aGCs had received more stimulation sessions, we found no differences between them and mice in the regular mature condition. Critically, we assessed remapping in both groups. Spatial

correlation between the first and last session was similar in days 1 and 0 in these 5 mice (left-tail Mann-Whitney days 1 vs. 0, p = 0.62). Similarly, there was no significant effect of mature aGC stimulation in animals belonging to the regular mature condition (left-tail Mann-Whitney days 1 vs. 0, p = 0.39). Given the similarities, data from the second round of experiments of these 5 mice was pooled into the mature condition.

During all OF sessions mice were filmed from a CCTV camera (sampling rate: 25 Hz) placed on the room ceiling. Animal position was tracked from green and red LEDs attached to the headstage (HS-18-MM-LED, Neuralynx, Inc., MT, USA). In all OF sessions chocolate cereal was sporadically scattered into the arena at random locations to encourage foraging. After every OF session, the surfaces of the arena were cleaned with 70% ethanol.

Familiarization (days −5 to −1): mice were familiarized with a single 15 min presentation to the same OF arena during 5 consecutive days.

Familiar environment experiments (days 0, 1 and 3): One, two and four days after the last familiarization day, multiple presentations of the same OF took place while CA3 single unit activity was recorded. Recording sessions included: a) 10 min rest in a pedestal outside the camera range, b) three consecutive OF sessions (15 min each) separated by 5 min resting periods in the pedestal and c) 10 min rest in the pedestal. In days 1 and 3, aGCs were optogenetically stimulated on session 2 in two epochs of 4 and 20 Hz (see below).

Novel environment experiment (day 2): the protocol was similar to the one for familiar environment experiments, but there were 4 sessions. Session 1 and 4 were conducted in the familiar environment, while sessions 2 and 3 were conducted in the novel environment. All OF sessions lasted 15 min and were separated by resting periods in the pedestal. The same cohort of aGCs was optogenetically stimulated on session 3 in two epochs of 4 and 20 Hz (see below). The protocol design for this day follows aims that are out of the scope of this manuscript and we do not analyze here maps in the novel environment.

Optical stimulation

Laser stimulation was performed using a 1 W, 447 nm laser (Tolket, Argentina). The light went through an SMA to ferrule rotary joint patch cable (Thorlabs, NJ, USA) and connected to the microdrive fiber optic ferrule with a quick-release interconnect (Thorlabs, NJ, USA). Laser intensity was modulated by an ISO-Flex optical isolator (AMPI, Israel) to achieve 30 mW measured before implantation surgery at the fiber-tip with a PM160T thermal sensor power meter (Thorlabs, NJ, USA).

Optical stimulation, controlled by an Arduino Uno (Arduino, MA, USA), consisted of 80 trains of 2-ms pulses (10 pulses per train) with 5 s of inter train interval. Total energy delivered per pulse was 60 μJ. The trains were divided in two epochs of 40 trains each, with a stimulation frequency of 4 and 20 Hz, respectively. The 4 and 20 Hz simulation epochs lasted approximately 300 s and 200 s, respectively. The 4 Hz epoch started after 2 min of OF exploration and there was an exploration time in between epochs of 160 s. In this way, the 20 Hz epoch ended 2 min before the end of the 15 min session.

Data collection

Single units activity (around 40 μV threshold) was acquired at a sampling rate of 32 kHz and filtered at 600 Hz to 6000 Hz using a Digital Lynx 4SX-M system (Neuralynx, Inc., MT, USA). Differential recordings were performed with a dedicated reference electrode in the cortex. Data processing was conducted with ad hoc MATLAB (MathWorks, MA, USA) scripts, as well as all subsequent analyses.

Spike sorting

Events corresponding to potential neural spikes were manually clustered offline. Multiple low dimensional projections were simultaneously used to identify well separated clusters: the peak-to-peak voltage in each channel, the voltage at user-defined time points of particular channels and two dimensional tSNE reductions with default parameters (MATLAB function *tsne*). Autocorrelation and cross-correlations were used as additional separation criteria.

Brain processing for histology

Electrodes were not moved after the final recording session. Subjects underwent an intraperitoneal injection of ketamine-xylazine anesthesia and were perfused intracardially with 100 mL of heparinized saline, and then with 100 mL of 4% paraformaldehyde. Three hours after perfusion, tetrodes were raised and the brain was extracted. It was stored in 4% paraformaldehyde overnight and then put in sucrose solution (30%) until it precipitated (around 48 h). Frozen coronal sections (40 μm) were cut with a microtome (Leica, Germany) and dorsal hippocampal sections were mounted on glass slides. After around 20-min drying, they were covered with PVA-DABCO mounting media and coverslips. The fluorescence microscopes BX60, Olympus (Japan; Figure S1B) and Examiner D1, ZEISS (Germany; Figure 1B) were used to obtain digitalized images.

Count of ChR2 expressing cells

Immunofluorescence: Eight-week-old Ascl1^{CreERT2} – CAG $^{flox\ Stop\ -\ ChR2\ EYFP}$ mice were injected intraperitoneally with TAM (120 μg/g) to achieve indelible expression of ChR2-EYFP in the cell membrane of aGCs (young: n = 4; mature: n = 4). Two injections were applied on a single day instead of four injections in two days (see above) to reduce expression, which facilitated soma discrimination by reducing cell overlap. After 4 (young condition) or 8 (mature condition) weeks, mice were sacrificed. Immunostaining was done on

40 μm free-floating coronal sections throughout the brain. Antibodies were applied in TBS with 3% donkey serum and 0.25% Triton X-100. Immunofluorescence was performed using anti GFP (chicken; 1:500; Aves Labs Inc., CA, USA). Donkey anti-chicken Cy2 was used as secondary antibody (1:250; Jackson ImmunoResearch Laboratories, PA, USA).

Confocal microscopy: One section per animal of the septal region of the hippocampus (anteroposterior, −1.5 to −2.2 mm from bregma) was included. Images were acquired using Zeiss LSM 5 Pascal confocal microscope (Carl Zeiss, Germany). Images were acquired (20×; NA 1.3) from 40-μm-thick sections, taking z-stacks, including typically x < 0.9 μm optical slices, airy unit = 1 at 1 μm intervals. Cell counting in the default z stack projection was restricted to cells with fluorescence intensity levels that enabled clear identification of their somata. Only $EYFP^+$ cells located in the granule cell layer and sub granule zone were included in the analysis (Figures S2A and S2B).

Ex vivo electrophysiology recordings

Slice Preparation: Eight-week-old $Ascl1^{CreERT2}$ – CAG $^{flox\ Stop\ -\ ChR2\ EYFP\ mice}$ were intraperitoneally anesthetized with ketamine-xylazine and decapitated 4 or 8 weeks after TAM induction. To prepare transverse slices, brains were removed into a chilled solution containing (in mM): 110 choline- Cl, 2.5 KCl, 2.0 NaH_2PO_4, 25 $NaHCO_3$, 0.5 $CaCl_2$, 7 $MgCl_2$, 20 dextrose, 1.3 Na^+-ascorbate, 3.1 Na^+-pyruvate, and 4 kynurenic acid (kyn). Coronal slices (400 μm thick) from the septal pole containing both hippocampi were cut with a vibratome and transferred to a chamber containing (in mM): 125 NaCl, 2.5 KCl, 2 NaH_2PO_4, 25 $NaHCO_3$, 2 $CaCl_2$, 1.3 $MgCl_2$, 1.3 Na^+-ascorbate, 3.1 Na^+-pyruvate, and 10 dextrose (315 mOsm). Slices were bubbled with 95% O_2/5% CO_2 and maintained at 30°C for ~45 min before experiments started.

Ex-Vivo Optogenetics: ChR2-expressing young or mature aGCs were stimulated using a 447×nm laser source delivered through the epifluorescence pathway of the upright microscope (FITC filter, 63× objective) commanded by the acquisition software. Loose-patch recordings were performed with ACSF-filled patch pipettes (8–10 MΩ) to record optically evoked currents (Figures 2C–2E).

QUANTIFICATION AND STATISTICAL ANALYSIS

Spatial maps

Spatial maps showing firing rate as a function of location were obtained by spatially smoothing (1.2 bin standard deviation 2D Gaussian filter) the ratio between spike count and time spent on a 2.5 cm side square bin grid covering all the arena.

Remapping was determined as the Pearson correlation between maps corresponding to two sessions, typically pre- and post stimulation, as indicated in each experiment. Non-covered spatial pixels were excluded for computing this and the other correlations.

Stability was computed as the Pearson correlation between maps constructed with either even or odd consecutive non-overlapping 30 s bins of each session. The total session length was segmented using 30 s bins. Mouse trajectory and single-unit activity data were grouped as falling in either even or odd bins. Maps were constructed for both groups and correlated to assess stability.

For population vector analyses maps were normalized by their mean. This ensured a purely spatial assessment of remapping, as when comparing cells individually through spatial correlation. The population vector was computed by concatenating the pixel values of all normalized spatial maps and all cells of a particular condition into a large vector. A single value, indicative of population remapping, was obtained by calculating the Pearson correlation between population vectors corresponding to two different sessions. Shuffling (see below) was used to assess statistical significance. For population vector analysis per mouse the same procedure was employed but now one PV value was obtained for each animal and then Mann-Whitney tests were performed to evaluated the statistical significance.

Spatial information rate for a spatial map with mean firing rate λ and a value λ_i for each of its N bins was computed as:

$$Information = \sum_{i=1}^{N} p_i \frac{\lambda_i}{\lambda} log_2\left(\frac{\lambda_i}{\lambda}\right)$$

where p_i is the occupancy probability of bin i.

Characterization of firing rate variation in stimulated bins

After noticing that the distribution of firing rates did not change due to stimulation in remapping or non-remapping cells, we computed for each cell the mean firing rate inside stimulated bins, normalized by the overall mean firing rate, using unsmoothed spatial maps (Figure S7). Stimulated bins were defined as those where at least one pulse of stimulation had occurred.

Shuffling statistics

Chance-level statistics was constructed for a given variable W (e.g., the population vector correlation) through a procedure of shuffling either the timestamps of events or the label of cells. For time shuffles, the entire sequence of spikes (Figures S1D and S1E) was time-shifted by a random interval between 30 s and the session duration minus 30 s, with the end of the session wrapped to the beginning. The shuffled instance of the variable W was then calculated using the shifted events (spikes or light pulses). The collection of 100 repetitions for each cell composed the chance-level statistics. To obtain cutoff values for cell classification, shuffled data for all cells were pooled together and the 95th percentile of the pooled distribution calculated.

Label shuffles were used to assess whether a single property W was different for two groups of cells. The shuffled distribution (10000 repetitions) for W was obtained by pooling all cells and re-grouping them randomly into groups of corresponding size. In each step, a new value of shuffled W was obtained, and the actual value of W was then compared with the shuffled distribution (Figures 1G, 3B, 3C, 4B, S8D, S8E, S8G, S11B–S11D and S11F).

Statistical analysis

Results were expressed as the median ± and the interquartile range (IQR) or the mean ± the standard error of the mean as indicated in each caption. Data were analyzed mainly through non-parametric statistics and the different tests (Kruskal-Wallis, Friedman's, Mann-Whitney and Wilcoxon), as well as their tails are indicated in each case. Tukey's honest significant difference criterion was employed as post-hoc test. In all cases, $p < .05$ was the statistical threshold. All analyses were carried out with MATLAB (MathWorks, MA, USA) using ad hoc scripts and the available built in functions.

Regarding left-tailed test to assess remapping, the rationale is that while familiarity takes correlations between maps obtained in consecutive sessions up, remapping drives correlations down. Since our experiments asked whether aGCs can induce remapping, one-tailed tests (left-tailed in this case) are the natural statistical tool.

Classification of patters of evoked activity

Histograms of the spiking of CA3 cells relative to single pulses of optical stimulation (−5 to 45 ms from light pulse onset) were considered as independent variables of a generalized linear model using a Poisson distribution (Figures S9C, S11A, 3A and 3B). Three categorical predictors corresponding to distinctive periods were included: baseline (−5 to 0 ms), early window (5–13 ms) and late window (15–30 ms). Significance of including early or late windows as predictors of cell activity was assessed.

Light-pulse train analysis

Evoked activity changes along the stimulation train were computed as the ratio between last and first pulses and comparing it against the hypothesis of a median equal to 1 (two tailed Wilcoxon test; Figure 3D). Only the early window (5–13 ms from light pulse onset) was considered.

Cell selection criteria

To analyze remapping, cells that were active and stable in the first session of each day were selected. This criterion was used because remapping can only be assessed on cells with stable spatial maps. Cells were considered active if the average firing rate in this session exceed 0.1 Hz. Cells were considered stable if the stability (see above) in this session exceed the 95th percentile of the shuffled distribution for that variable. Cells were considered putative fast spiking if their average firing rate during this session was above 7 Hz and putative pyramidal otherwise. Putative fast spiking cells were excluded from the analysis of remapping.

Percentage of active and stable putative pyramidal cells from total recorded: 155/370 (42%).
Per condition (Young and Mature): 93/212 (44%), 62/158 (39%).
Per day (1–4):
young: 18/50 (36%), 35/80 (44%), 24/52 (46%), 16/30 (53%).
mature: 21/56 (38%), 22/57 (39%), 11/30 (37%), 8/15 (53%).